
Stateless actor-critic for instance segmentation with high-level priors

Paul Hilt

Cell Biology and Biophysics Unit
European Molecular Biology Laboratory
paul.hilt@embl.de

Edgar Kaziakhmedov

Cell Biology and Biophysics Unit
European Molecular Biology Laboratory
Skolkovo Institute of Science and Technology
edgar.kaziakhmedov@phystech.edu

Sourabh Bhide

Director's Research
European Molecular Biology Laboratory
sourabh.bhide@embl.de

Maria Leptin

Director's Research
European Molecular Biology Laboratory
European Molecular Biology Organization
maria.leptin@embo.org

Constantin Pape

Cell Biology and Biophysics Unit
European Molecular Biology Laboratory
constantin.pape@embl.de

Anna Kreshuk

Cell Biology and Biophysics Unit
European Molecular Biology Laboratory
anna.kreshuk@embl.de

Abstract

Instance segmentation is an important computer vision problem which remains challenging despite impressive recent advances due to deep learning-based methods. Given sufficient training data, fully supervised methods can yield excellent performance, but annotation of ground-truth data remains a major bottleneck, especially for biomedical applications where it has to be performed by domain experts. The amount of labels required can be drastically reduced by using rules derived from prior knowledge to guide the segmentation. However, these rules are in general not differentiable and thus cannot be used with existing methods. Here, we relax this requirement by using stateless actor critic reinforcement learning, which enables non-differentiable rewards. We formulate the instance segmentation problem as graph partitioning and the actor critic predicts the edge weights driven by the rewards, which are based on the conformity of segmented instances to high-level priors on object shape, position or size. The experiments on toy and real datasets demonstrate that we can achieve excellent performance without any direct supervision based only on a rich set of priors.

1 Introduction

Instance segmentation is the task of segmenting all objects in an image and assigning each of them a different label. It forms the necessary first step to the analysis of individual objects in a scene and is thus of paramount importance in many practical applications of computer vision. Over the recent years, fully supervised instance segmentation methods have made tremendous progress both in natural image applications and in scientific imaging, achieving excellent segmentations for very difficult tasks [1, 2].

A large corpus of training images is hard to avoid when the segmentation method needs to take into account the full variability of the natural world. However, in many practical segmentation

tasks the appearance of the objects can be expected to conform to certain rules which are known *a priori*. Examples include surveillance, industrial quality control and especially medical and biological imaging applications where full exploitation of such prior knowledge is particularly important as the training data is sparse and difficult to acquire: pixelwise annotation of the necessary instance-level groundtruth for a microscopy experiment can take weeks or even months of expert time. The use of shape priors has a strong history in this domain [3, 4], but the most powerful learned shape models still require groundtruth [5] and generic shapes are hard to combine with the CNN losses and other, non-shape, priors. For many high-level priors it has already been demonstrated that integration of the prior directly into the CNN loss can lead to superior segmentations while significantly reducing the necessary amounts of training data [6]. However, the requirement of formulating the prior as a differentiable function poses a severe limitation on the kinds of high-level knowledge that can be exploited with such an approach. The aim of our contribution is to address this limitation and establish a framework in which a rich set of non-differentiable rules and expectations can be used to steer the network training.

To circumvent the requirement of a differentiable loss function, we turn to the reinforcement learning paradigm, where the rewards can be computed from a non-differentiable cost function. We base our framework on a stateless actor-critic setup [7], providing one of the first practical applications of this important theoretical construct. In more detail, we solve the instance segmentation problem as agglomeration of image superpixels, with the agent predicting the weights of the edges in the superpixel region adjacency graph. Based on the predicted weights, the segmentation is obtained through (non-differentiable) graph partitioning and the segmented objects are then evaluated by the critic, which learns to approximate the rewards based on the object- and image-level reasoning (see Fig. 1).

The main contributions of this work can be summarized as follows: (i) we formulate instance segmentation as a RL problem based on a stateless actor-critic setup, encapsulating the non-differentiable step of instance extraction into the environment and thus achieving end-to-end learning; (ii) we exploit prior knowledge on instance appearance and morphology by tying the rewards to the conformity of the predicted objects to pre-defined rules and learning to approximate the (non-differentiable) reward function with the critic; (iii) we introduce a strategy for spatial decomposition of rewards based on fixed-sized subgraphs to enable localized supervision from combinations of object- and image-level rules. (iv) we demonstrate the feasibility of our approach on synthetic and real images and show an application to an important segmentation task in developmental biology, where our framework delivers an excellent segmentation with no supervision other than high-level rules.

2 Related work

Reinforcement learning has so far not found significant adoption in the segmentation domain. The closest to our work are two methods in which RL has been introduced to learn a sequence of segmentation decision steps as a Markov Decision Process. In the actor critic framework of [8], the actor recurrently predicts one instance mask at a time based on the gradient provided by the critic. The training needs fully segmented images as supervision and the overall system, including an LSTM sub-network between the encoder and the decoder, is fairly complex. In [9], the individual decision steps correspond to merges of clusters while their sequence defines a hierarchical agglomeration process on a superpixel graph. The reward function is based on Rand index and thus not differentiable, but the overall framework requires full (super)pixelwise supervision for training.

Reward decomposition was introduced for multi agent RL by [10] where a global reward is decomposed into a per agent reward. [11] proves that a stateless RL setup with decomposed rewards requires far less training samples than a RL setup with a global reward. In [12] reward decomposition is applied both temporally and spatially for zero-shot inference on unseen environments by training on locally selected samples to learn the underlying physics of the environment.

The restriction to differentiable losses is present in all application domains of deep learning. Common ways to address it are usually based on a soft relaxation of the loss that can be differentiated. The relaxation can be designed specifically for the loss, such as, for example, Area-under-Curve [13] for classification or Jaccard Index [14] for semantic segmentation. These approaches are not directly applicable to our use case as we aim to enable the use of a variety of object- and image-level priors which can easily be combined without handcrafting an approximate loss for each case. More generally, but still for a concrete task loss, Direct Loss Minimization has been proposed for CNN training in [15]. For semi-supervised learning of a classification or ranking task, Discriminative Adversarial

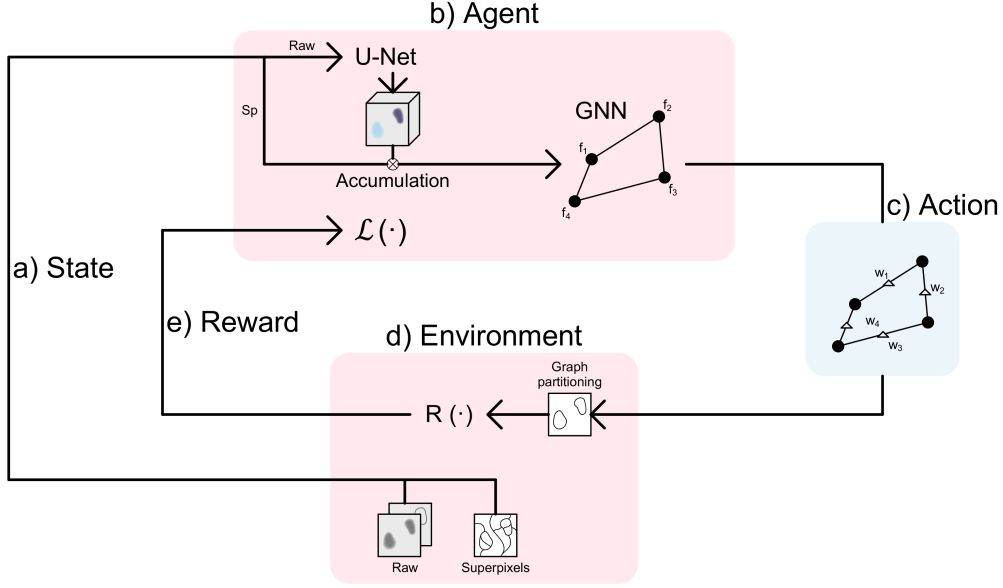


Figure 1: Interaction of the agent with the environment: (a) shows the state which is composed of the raw image and the superpixel over-segmentation; (b) depicts the agent and the superpixel graph, which accumulates the features for nodes of the GNN from pixels which belong to the corresponding superpixels; (c) given the state, the agent performs the actions by predicting edge weights on the superpixel graph; (d) the environment, which includes the graph partitioning built from the weights predicted through agent actions; (e) rewards are obtained by evaluating the segmentation arising from the graph partitioning, based on pre-defined and data dependent rules. The rewards are given back to the agent where they are used for training.

Networks have been proposed as a means to learn an approximation to the loss [16]. Most generally, Grabocka et al. in [17] propose to train a surrogate neural network which will serve as a smooth approximation of the true loss. In our setup, the critic can informally be viewed as a surrogate network as it learns to approximate the priors through the rewards by Q-learning.

Incorporation of rules and priors is particularly important in biomedical imaging applications, where such knowledge can be exploited to augment or even substitute scarce groundtruth annotations. For example, the shape prior is explicitly encoded in the popular nuclear [18] and cellular [19] segmentation algorithms based on spatial embedding learning. Learned non-linear representations of the shape are used in [5], while in [20] the loss for object boundary prediction is made topology-aware. Domain-specific priors can also be exploited in post-processing by graph partitioning [21]. Interestingly, the energy minimization procedure underlying the graph partitioning can also be incorporated into the learning step [22, 23].

3 Methods

The task of instance segmentation can be formalized as transforming an image x into a labeling y , where y maps each pixel to a label value. An instance corresponds to the maximal set of pixels with the same label value. Typically, the instance segmentation problem is solved via supervised learning, i.e. using a training set with ground-truth labels \hat{y} . Note that y is invariant under the permutation of label values. In general, it is difficult to formulate instance segmentation in a fully differentiable manner. Most approaches first predict a "soft" representation with a CNN, e.g. affinities [1, 24, 25], boundaries [26, 27] or embeddings [28, 29] and apply non-differentiable post-processing, such as agglomeration [27, 30], clustering [31, 32] or partitioning [33], to obtain the instance segmentation. Alternatively, proposal-based methods predict a bounding-box per instance and then predict the instance mask for each bounding-box [34]. Furthermore, the common evaluation metrics for instance segmentation [35, 36] are also not differentiable.

Our main motivation to explore RL for the instance segmentation task is to circumvent the restriction to differentiable losses and - regardless of the loss - to make the whole pipeline differentiable end-to-

end even in presence of non-differentiable steps which transform pixelwise CNN predictions into individual instances.

We formulate the instance segmentation problem using a region adjacency graph $G = (V, E)$, where the nodes V correspond to superpixels (homogeneous clusters of pixels) and the edges E connect nodes which belong to spatially adjacent superpixels. Given edge weights W , an instance segmentation can be obtained by partitioning the graph, here using an approximate multicut solver [37]. Together, the image data, superpixels, graph and the graph partitioning make up the environment \mathcal{E} of our RL setup. Based on the state s of \mathcal{E} , the agent \mathcal{A} predicts actions a , which are used to compute the partitioning. The reward r is then computed based on this partitioning. Our agent \mathcal{A} is a stateless actor-critic [38], represented by two graph neural networks (GNN) [39]. The actor predicts the actions a based on the graph and its node features F . The node(superpixel) features are computed by pooling together the corresponding pixel features based on the raw image data.

Here, we make use of two different setups: Method 1, where the per-pixel features are computed based on the image data with the feature extractor being part of the agent \mathcal{A} and Method 2 where the feature extractor is part of the environment \mathcal{E} . The feature extractor is trained end-to-end in Method 1, whereas it is fixed and thus needs to be pre-trained in Method 2. We use a U-Net [40] as feature extractor and can use hand-crafted features in addition to the learned features. More details about the pre-training can be found in the Appendix A.2. The agent - environment interaction for Method 1 is depicted in Figure 1. For Method 2 we refer to the Appendix A.1.

Importantly, this setup enables us to use both a non-differentiable instance segmentation step and reward function, by encapsulation of the “pixels to instances” step in the environment and learning a policy based on the rewards with a stateless actor critic.

3.1 Stateless Reinforcement Learning Setup

Unlike most RL settings [41], our approach does not require an explicitly time dependent state: the actions returned by the agent correspond to the real-valued edge weights in $[0, 1]$, which are used to compute the graph partitioning. Any state can be reached by a single step from the initial state and there exists no time dependency in the state transition. Unlike [9], we predict all edge values at once which allows us to avoid the iterative strategy of [8] and deliver and evaluate a complete segmentation in every step. We implement a stateless actor critic formulation with episodes of length 1.

To the best of our knowledge, stateless RL was introduced in [7] to study the connection between generative adversarial networks and actor critics and our method is one of the first practical applications of this concept. Here, the agent consists of an actor, which predicts the actions a and a critic, which predicts the action value Q (expected future discounted reward) given the actions. The stateless approach simplifies the action value function: the action value has to estimate the reward for a single step instead of estimating the expected sum of discounted future rewards for many steps. We have explored a multi-step setup as well, but found that it yields inferior results for our application; details can be found in the Appendix A.9. As described in detail in Subsection A.8, we compute localized sub-graph rewards instead of relying on a single global reward.

The actor corresponds to a single GNN, which predicts the mean and variance of a normal distribution for each edge. The actions a are determined by sampling from this distribution and applying a sigmoid to the result to obtain continuous edge weights in the value range $[0, 1]$. The GNN takes the state $s = (G, F)$ as input arguments and its graph convolution for the i^{th} node is defined as in [39]:

$$f_i = \gamma_\pi \left(f_i, \frac{1}{|N(i)|} \sum_{j \in N(i)} \phi_\pi(f_i, f_j) \right) \quad (1)$$

where γ_π as well as ϕ_π are MLPs, (\cdot, \cdot) is the concatenation of vectors and $N(i)$ is the set of neighbors of node i . The gradient of the loss for the actor is given by:

$$\nabla_\theta \mathcal{L}_{actor} = \nabla_\theta \frac{1}{|SG|} \sum_{sg \in G} \left[\alpha \sum_{\hat{a} \in sg} \log(\pi^\theta(\hat{a}|s)) - Q_{sg}(s, a) \right] \quad (2)$$

This loss gradient is derived following [38]. We adapt it to the sub-graph reward structure by calculating the joint action probability of the policy π^θ over each sub-graph sg in the set of all sub-graphs SG . Using this loss to optimize the policy parameters θ minimizes the Kullback-Leibler

divergence between the Gibbs distribution of action values for each sub-graph $Q_{sg}(s, a)$ and the policy with respect to the parameters θ of the policy. α is a trainable temperature parameter which is optimized following the method introduced by [38].

The critic predicts the action value Q_{sg} for each sub-graph $sg \in SG$. It consists of a GNN $Q_{sg}(s, a)$ that takes the state $s = (G, F)$ as well as the actions a predicted by the actor as input and predicts a feature vector for each edge. The graph convolution from Equation 2 is slightly modified:

$$f_i = \gamma_Q \left(f_i, \frac{1}{|N(i)|} \sum_{j \in N(i)} \phi_Q(f_i, f_j, a_{(i,j)}) \right) \quad (3)$$

again γ_Q and ϕ_Q are MLPs. Based on these edge features Q_{sg} is predicted for each sub-graph via an MLP. Here, we use a set of subgraph sizes (typically, 6, 12, 32, 128) to generate a supervision signal for different neighborhood scales. A given MLP is only valid for a fixed graph size, so we employ a different MLP for each size. The loss for the critic is given by:

$$\mathcal{L}_{critic} = \frac{1}{|SG|} \sum_{sg \in G} \frac{1}{2} (Q_{sg}^\delta(s, a) - r)^2 \quad (4)$$

Minimizing this loss with respect to the action value function’s parameters δ minimizes the difference between the expected reward and action values $Q_{sg}^\delta(s, a)$.

3.2 Localized Supervision Signals

The RL paradigm is to provide a global reward for a given state transition [41]. However, we find that for our application it is possible and desirable to instead provide several more localized rewards per state transition: Given a large action space with a policy represented by a complex multivariate probability distribution, it is beneficial to learn from rewards for the specific actions rather than from a scalar global reward for the union of all actions. Of course then requirement arises that the union of local rewards must resemble to the global reward. E.g. the optimal policy is the same for local as for the global reward.

Our actor critic setup (Section 3.1) expects rewards per sub-graph. A good set of sub-graphs should fulfill the following requirements: each sub-graph should be connected so that the information presented to the MLP computing the action value for this sub-graph is correlated. The size of the sub-graphs, given by the number of edges, should be a parameter and all sub-graphs should be extracted with exactly that size to serve as valid input for one of the MLPs. The union of all sub-graphs should cover the complete graph so that each edge contributes to at least one action value Q_{sg} . The sub-graphs should overlap to provide a smooth sum of action values. We introduce Algorithm 1 to extract such a set of sub-graphs (see Appendix A.8). Figure 2 shows the sub-graphs for a small example graph.

While some of the rewards used in our experiments can be directly defined for the sub-graphs, most are instead defined per object (see Appendix A.3 for details on reward design). We use the following general procedure to map object-level rewards to sub-graphs: first assign to each superpixel the reward of its corresponding object, then determine the reward per edge as the maximum value of its two incident superpixels’ rewards and average the edge rewards to obtain the reward per sub-graph. Here, we use the maximum because high object scores indicate that all actions contributing to the respective object should get a high reward. However, for low object scores it is not possible to localize the specific action responsible for the low score. Hence, by taking the maximum we assign the higher score to edges whose incident superpixels belong to different objects, because they probably correspond to a correct split. Note that the uncertainty in the assignment of low rewards can lead to a noisy reward signal, but the averaging of the edge rewards over the sub-graphs and the overlaps between the sub-graphs smooth and partially denoise the rewards. We have also explored a different actor critic setup that can use object level rewards directly, eliminating the need for the sub-graph extraction and mapping. However, this approach yields inferior results, see the Appendix A.4 for details.

4 Experiments

The agent of our setup acts on the superpixel graph and thus depends on the features assigned to the nodes of the graph. We introduced two variants of our algorithm: in the base variant (Method 1)

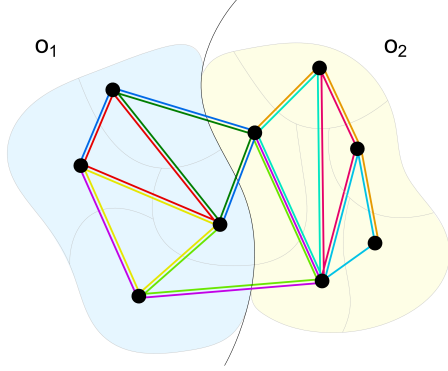


Figure 2: The graph is subdivided into sub-graphs, each sub-graph is highlighted by a different color. All sub-graphs have the same number of edges (here 3). Overall, we use a variety of sizes covering different notions of locality.

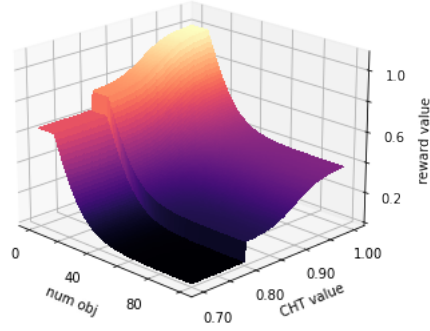


Figure 3: An example reward landscape Circle Hough Transform (CHT) rewards. High rewards are given if the overall number of predicted objects is not too high and if the respective object has a large CHT value. We found an exponential gradient of the reward landscape to work best.

we start from random features and make them part of the agent, allowing them to change through back-propagation (Fig. 1). In contrast, Method 2 acts on predefined features which are provided as part of the environment and are computed before training, e.g. through unsupervised clustering. A very accurate clustering in the features produces an easy problem for the agent to solve where even a global reward for all actions might be sufficient. However, in a real-world setting with no supervision, the noisier the features become the more local the reward has to be. We evaluate Method 2 on synthetic data where self-supervised pretraining can deliver noisy, but meaningful node features. Our full setup with Method 1 is evaluated on a dataset from a light microscopy experiment, where highly regular object shapes are to be expected, but no good feature pre-training is possible.

To transform the edge weight predictions of the agent into an instance segmentation we use the Multicut [42] algorithm. Here, other options are also possible such as hierarchical clustering used in [9], but we choose the Multicut for its global optimality property. Hyperparameters of the pipeline were found by cross-validation (see Appendix A.10). We use [43] for visualization of all experimental setups.

4.1 Synthetic dataset: circles on structured ground

To evaluate the feasibility of our approach, we create a synthetic dataset with prominent structured background. Our aim is to segment irregular disks on such background using only rule-based supervision. We generate the superpixels by the mutex watershed algorithm [25] which we run on the Gaussian gradient image. The node features of the superpixel graph were computed through self-supervised pretraining with contrastive loss as described in Appendix A.2 and fixed as part of the environment.

As we aim to segment disks, we compute the circularity of the segmented objects for the rewards using the Circle Hough Transform [44]. This object-level reward is combined with the global rough estimate of the number of objects in the image to create the reward surface depicted in Fig. 3. The reward for the number of objects provides useful gradient during early training stages: for example, when too few potential objects are found in the prediction, a low reward can be given to what is thought to be the background object. On the other hand, if too many potential objects are found, a low reward can be given to all the foreground objects with a low CHT value.

In more detail, the object rewards r_{fg} are composed as follows. We define a threshold γ on the CHT value ($\gamma = 0.8$ in the reward surface shown in Fig. 3). Let $c \in [0, 1]$ be the CHT value corresponding to the object and let k be the total number of objects that we expect and n be the number of predicted objects. Then

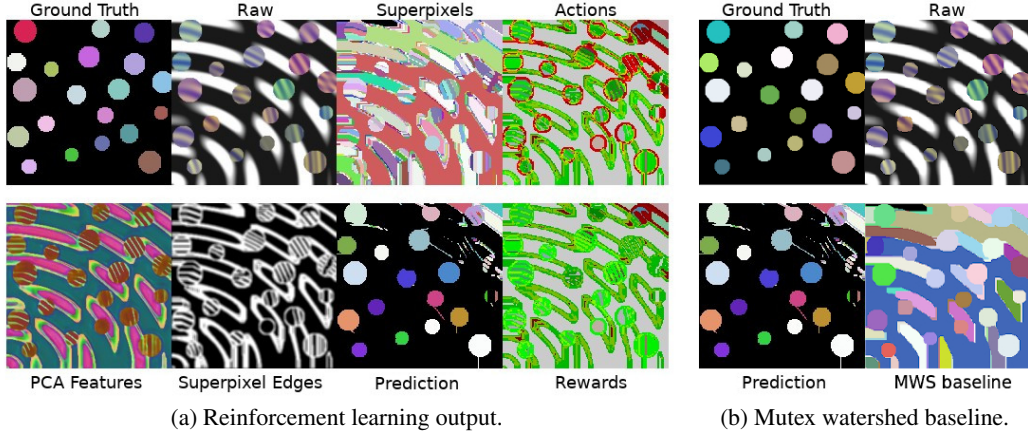


Figure 4: The “Circles” dataset. Top left to right: ground truth segmentation, raw data, superpixel over-segmentation and a visualizaatoin for the actions on every edge, where a merge action is displayed in green and a split action in red. Bottom left to right: the pre-trained pixel embeddings projected to their first 3 PCA components shown as RGB, an edge image of the superpixels, the segmentation resulting from the graph agglomeration on the predicted edge weights and a visualization of the rewards based on the CHT, where light green shows high rewards and dark red low rewards.

$$r_{local} = \begin{cases} \sigma \left(\left(\frac{c-\gamma}{1-\gamma} - 0.5 \right) 6 \right) 0.4, & \text{if } c \geq \gamma \\ 0, & \text{otw} \end{cases} \quad (5)$$

$$r_{global} = \begin{cases} r_{exp} \left(\frac{k}{n} \right), & \text{if } n \geq k \\ 0.6, & \text{otw} \end{cases} \quad (6)$$

$$r_{fg} = r_{local} + r_{global} \quad (7)$$

Here $\sigma(\cdot)$ is the sigmoid function. The input to the sigmoid function is normalized to the interval $[-3, 3]$ which was empirically found to be a good range. The rewards are always in $[0, 1]$ here this is split up into $[0, 0.5]$ for the local reward as well as for the global reward.

For the largest predicted object we strongly suspect the background object. For this object background rewards r_{bg} are calculated by

$$r_{bg} = \begin{cases} r_{exp} \left(\frac{n}{k} \right), & \text{if } n \leq k \\ 1, & \text{otw} \end{cases} \quad (8)$$

Note that this rewards have a large globally calculated part which makes this setup not fit for Method 1. It needs some feature representation that already gives a good idea for the clustering. The only useful local information in the reward is the CHT value. Therefore, if the features have a fairly distinct structure for circles, the agent should be able to find and to correctly cluster them.

Fig. 4 shows the output of all algorithm components on a sample image. For comparison, we also computed mutex watershed [25] predictions. Texture within objects and structured background are inherently difficult for region-growing algorithms, but our approach can exploit higher-level reasoning along with low-level information and achieve a good segmentation.

4.2 Real dataset: light microscopy imaging

Biomedical applications often require segmentation of objects of known morphology which are positioned in regular patterns, while extensive prior knowledge is available on variability of both under normal experimental conditions [45]. Such data presents the best use case for our algorithm as the reward function can leverage the known characteristics of individual object shape and texture and the overall similarity of the objects.

The dataset used for this experiment contains 317 2D images extracted from a video of a developing fruitfly embryo acquired with a light-sheet microscope [46] (Fig. 5). The image shows boundaries (plasma membranes) of the embryo cells. Across the dataset, 10 images were fully segmented by an expert, we use those for validation.

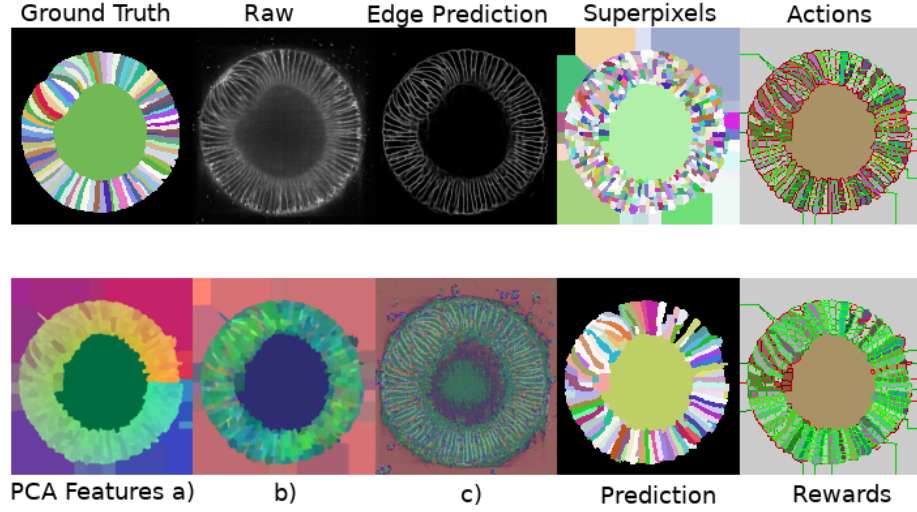


Figure 5: Microscopy dataset experiment. Top left to right: ground truth segmentation; raw data; edge map; superpixel over-segmentation; visualization for the actions on every edge, where a merge action is displayed in green and a split action in red. Bottom left to right: a) handcrafted features; b) learned features accumulated on superpixels; c) learned features projected to their first 3 PCA components shown as RGB; the segmentation resulting from the Multicut on the predicted edge weights; visualization of the rewards, where light green shows high rewards and dark red low rewards.

Fruitfly embryo is a well-studied system for which we can exploit the prior knowledge on the expected cell shape and the radial pattern of cells. Furthermore, as the analysis of cell shape dynamics is a paramount part of many biological experiments, multiple pre-trained networks are available for the cell segmentation task [18, 19, 47, 48]. Due to the differences in sample preparation and image acquisition settings, none of these would work out-of-the-box for our data. However, the CNNs in [48] which are trained to predict boundaries in confocal microscope images of plant tissue, can serve as a strong edge detector to create superpixels in our images. The superpixels are obtained using the seeded watershed algorithm on seeds at the local minima of the predicted edge map.

The rewards for this experiment are designed as follows: we set a high reward for merging the superpixels which are certain to lie in the background (close to the image boundary or the image center). For the background edges near the foreground area we modulate the reward by the circularity of the overall foreground contour. Finally, for the edges which are likely to be in the foreground we compute object-level rewards by fitting a rotated bounding box to each object and comparing its side lengths as well as its orientation to predefined template values. We do not perform semantic segmentation to define precise foreground/background boundaries, but instead use a soft weighting scheme with Gaussian weights to combine object and background rewards based on the prior knowledge of the embryo width. An image of the weights for different locations in the image can be found in the Appendix A.7 .

More formally the edge rewards r_{edge} are calculated as follows. For each edge, we define the distance h between the edge and the center of the image as the average distance of the incident objects' center of mass and the center c of the image. j is the approximate radius of the circle that lies within the foreground and m is the maximal distance between c and the image boarder. Let further $\mathcal{K}(\cdot)$ be the Gaussian kernel function. Then r_{edge} yields

$$r_{bg} = \begin{cases} \mathcal{K}\left(\frac{\|h-c\|}{\gamma}\right) (1-a), & \text{if } h \leq j \\ \mathcal{K}\left(\frac{\|m-h\|}{\eta}\right) (1-a), & \text{otw} \end{cases} \quad (9)$$

$$r_{fg} = \mathcal{K}\left(\frac{\|h-j\|}{\delta}\right) \max(r_{o1}, r_{o2}) \quad (10)$$

$$r_{edge} = r_{fg} + r_{bg} \quad (11)$$

Table 1: Quantitative evaluation on the microscopy dataset. Note that the projection of superpixels to the ground truth (sp gt) sets an upper (lower for VI) bound for our method. We use Symmetric Best Dice as well as the Variation of Information metric to compare all results on the validation set.

Method	SBD	VI merge	VI split
sp gt	0.656 ± 0.019	0.672 ± 0.061	0.594 ± 0.028
ours + augmentation noise	0.508 ± 0.031	1.233 ± 0.156	1.060 ± 0.258
ours	0.482 ± 0.020	0.839 ± 0.118	1.374 ± 0.357
ours without edges	0.446 ± 0.041	0.953 ± 0.212	0.994 ± 0.200
ours only handcrafted	0.408 ± 0.087	0.987 ± 0.101	1.536 ± 0.410
edge + mc [48]	0.283 ± 0.023	3.019 ± 0.040	0.342 ± 0.045
contrastive [28]	0.215 ± 0.009	1.155 ± 0.037	3.285 ± 0.084
contrastive + edge [28]	0.248 ± 0.014	1.229 ± 0.048	3.336 ± 0.073

Here γ, η, δ are normalization constants. Equation 9 first determines the background probability for an edge by the kernel values. $1 - a$ constitutes a reward that directly favors merges which is scaled by the background probability. For each edge, r_{o1} and r_{o2} are the rewards corresponding to the two objects connected to that edge. The object rewards are given by fitting a rotated bounding box to the object and then compare rotation and dimensions to template values.

Note that in this experiment no self-supervised pretraining is used for the node features in the agent’s GNNs. Unlike the “Circles” dataset, all objects in these images have very similar intensity distributions and can only be separated through the detection of boundaries between them. Instead of the pretraining, we experiment with using a few hand-crafted features like the polar coordinate of the node’s respective superpixel’s center of mass with respect to the coordinate system sitting at the center of the image as well as the superpixel’s mass, and with learning other features by back-propagation from the agent. The handcrafted features are normalized, concatenated to the learned features and used as input to the GNN. The projection of the first 3 PCA components of these features into RGB space is shown in Fig. 5 respectively for learned feature maps, their projection to node features through the accumulation procedure and finally the concatenation of those and the handcrafted features. Note that the learned features converge to a representation which resembles a semantic segmentation of boundaries in the image.

We train the complete setup for Method 1 end-to-end on a Nvidia GeForce RTX 3090 GPU for 4 days. For comparison we keep the model which achieved the highest reward on the test set. This makes training as well as the validation independent from ground truth annotations. The evolution of the rewards on the validation set for different random seeds is shown in the Appendix A.6. All of the conducted trainings show a stride for high rewards regardless of different random seeding.

For the validation scores we use the variation of information (VI) for both input combinations (merge and split) and the Symmetric Best Dice score. To show the influence of the imperfect superpixels on the final clustering, we project the superpixels to their respective ground truth clustering (“sp gt” in Table 1) which sets an upper (lower in case of VI) bound for our method. In this study we use several versions of our approach. In Table 1 (ours) refers to method 1 as described in section 4.2, (ours + augmentation noise) is the same method but add some noise to the input data during training, (ours without edges) is our method but without the additional edge prediction as an input and (ours only handcrafted) is our method where we only use the handcrafted features as described in section 4.2. We find that learned features significantly contribute to the performance of our method.

We compare to the following baseline approaches: *edge + mc*, which solves the Multicut graph partitioning based on edge weights derived from boundary predictions used for superpixel creation, *contrastive*, which predicts a pixel-wise embedding space that is clustered into instances using k-means and for which the embeddings are trained using the discriminative loss function of [28] on the ovules dataset from [48] and *contrastive + edge*, which is similar to *contrastive*, but receives the [48] boundary predictions as additional input channel.

5 Discussion

We introduced an end-to-end instance segmentation algorithm which can exploit non-differentiable loss functions and high-level prior information. Our RL approach is based on stateless actor-critic

and predicts the full segmentation at every step, allowing us to assign rewards to all objects and reach stable convergence. The segmentation problem is formulated as graph partitioning; we design a reward decomposition algorithm which maps object- and image-level rewards to sub-graphs for localized supervision.

We performed proof-of-concept experiments to demonstrate the feasibility of our approach on synthetic and real data and showed in particular that our setup can segment microscopy images with no direct supervision other than high-level reasoning. In the future, we plan to explore other problems and reward functions as well as a semi-supervised setup (briefly introduced in Appendix A.11) where we think our approach can be very beneficial. Furthermore, even in case of full supervision with ample groundtruth, our RL-based formulation enables end-to-end instance segmentation with direct object-level reasoning, which will allow for post-processing-aware training of the CNN which predicts object boundaries or embeddings.

References

- [1] Kisuk Lee, Jonathan Zung, Peter Li, Viren Jain, and H. Sebastian Seung. Superhuman accuracy on the snemi3d connectomics challenge, 2017.
- [2] Liang-Chieh Chen, Huiyu Wang, and Siyuan Qiao. Scaling wide residual networks for panoptic segmentation, 2021.
- [3] S. Osher and N. Paragios. *Geometric Level Set Methods in Imaging, Vision, and Graphics*. Springer New York, 2007. ISBN 9780387218106. URL <https://books.google.de/books?id=ZWzrBwAAQBAJ>.
- [4] Ricard Delgado-Gonzalo, Virginie Uhlmann, Daniel Schmitter, and Michael Unser. Snakes on a plane: A perfect snap for bioimage analysis. *IEEE Signal Processing Magazine*, 32(1):41–48, 2014.
- [5] Ozan Oktay, Enzo Ferrante, Konstantinos Kamnitsas, Mattias Heinrich, Wenjia Bai, Jose Caballero, Stuart A. Cook, Antonio de Marvao, Timothy Dawes, Declan P. O’Regan, Bernhard Kainz, Ben Glocker, and Daniel Rueckert. Anatomically constrained neural networks (acnns): Application to cardiac image enhancement and segmentation. *IEEE Transactions on Medical Imaging*, 37(2):384–395, 2018. doi: 10.1109/TMI.2017.2743464.
- [6] Hoel Kervadec, Jose Dolz, Meng Tang, Eric Granger, Yuri Boykov, and Ismail Ben Ayed. Constrained-cnn losses for weakly supervised segmentation. *Medical Image Analysis*, 54:88–99, 2019. ISSN 1361-8415. doi: <https://doi.org/10.1016/j.media.2019.02.009>.
- [7] David Pfau and Oriol Vinyals. Connecting generative adversarial networks and actor-critic methods. *CoRR*, abs/1610.01945, 2016. URL <http://arxiv.org/abs/1610.01945>.
- [8] Nikita Araslanov, Constantin Rothkopf, and Stefan Roth. Actor-critic instance segmentation. In *Proceedings of the IEEE Conference on Computer Vision and Pattern Recognition (CVPR)*, 2019.
- [9] Viren Jain, Srinivas Turaga, Kevin Briggman, Moritz Helmstaedter, Winfried Denk, and Hyun-june Seung. Learning to agglomerate superpixel hierarchies. *Advances in Neural Information Processing Systems*, 24, 01 2011.
- [10] Peter Sunehag, Guy Lever, Audrunas Gruslys, Wojciech Marian Czarnecki, Vinicius Zambaldi, Max Jaderberg, Marc Lanctot, Nicolas Sonnerat, Joel Z. Leibo, Karl Tuyls, and Thore Graepel. Value-decomposition networks for cooperative multi-agent learning, 2017.
- [11] Drew Bagnell and Andrew Ng. On local rewards and scaling distributed reinforcement learning. In Y. Weiss, B. Schölkopf, and J. Platt, editors, *Advances in Neural Information Processing Systems*, volume 18. MIT Press, 2006. URL <https://proceedings.neurips.cc/paper/2005/file/02180771a9b609a26dcea07f272e141f-Paper.pdf>.
- [12] Huazhe Xu, Boyuan Chen, Yang Gao, and Trevor Darrell. Scoring-aggregating-planning: Learning task-agnostic priors from interactions and sparse rewards for zero-shot generalization. *CoRR*, abs/1910.08143, 2019. URL <http://arxiv.org/abs/1910.08143>.

- [13] Elad Eban, Mariano Schain, Alan Mackey, Ariel Gordon, Ryan Rifkin, and Gal Elidan. Scalable learning of non-decomposable objectives. In *Artificial intelligence and statistics*, pages 832–840. PMLR, 2017.
- [14] Maxim Berman, Amal Rannen Triki, and Matthew B Blaschko. The lovász-softmax loss: A tractable surrogate for the optimization of the intersection-over-union measure in neural networks. In *Proceedings of the IEEE Conference on Computer Vision and Pattern Recognition*, pages 4413–4421, 2018.
- [15] Yang Song, Alexander G. Schwing, Richard S. Zemel, and Raquel Urtasun. Training deep neural networks via direct loss minimization. *International Conference on Machine Learning*, 2016.
- [16] Cicero Nogueira dos Santos, Kahini Wadhawan, and Bowen Zhou. Learning loss functions for semi-supervised learning via discriminative adversarial networks, 2017.
- [17] Josif Grabocka, Randolph Scholz, and Lars Schmidt-Thieme. Learning surrogate losses. *arXiv preprint arXiv:1905.10108*, 2019.
- [18] Uwe Schmidt, Martin Weigert, Coleman Broaddus, and Gene Myers. Cell detection with star-convex polygons. In *International Conference on Medical Image Computing and Computer-Assisted Intervention*, pages 265–273. Springer, 2018.
- [19] Carsen Stringer, Tim Wang, Michalis Michaelos, and Marius Pachitariu. Cellpose: a generalist algorithm for cellular segmentation. *Nature Methods*, 18(1):100–106, 2021.
- [20] Xiaoling Hu, Fuxin Li, Dimitris Samaras, and Chao Chen. Topology-preserving deep image segmentation. In *Advances in Neural Information Processing Systems*, volume 32, 2019. URL <https://proceedings.neurips.cc/paper/2019/file/2d95666e2649fcfc6e3af75e09f5adb9-Paper.pdf>.
- [21] Constantin Pape, Alex Matskevych, Adrian Wolny, Julian Hennies, Giulia Mizzon, Marion Louveaux, Jacob Musser, Alexis Maizel, Detlev Arendt, and Anna Kreshuk. Leveraging domain knowledge to improve microscopy image segmentation with lifted multicuts. *Frontiers in Computer Science*, 1:6, 2019.
- [22] Jeremy B Maitin-Shepard, Viren Jain, Michal Januszewski, Peter Li, and Pieter Abbeel. Combinatorial energy learning for image segmentation. In D. Lee, M. Sugiyama, U. Luxburg, I. Guyon, and R. Garnett, editors, *Advances in Neural Information Processing Systems*, volume 29. Curran Associates, Inc., 2016. URL <https://proceedings.neurips.cc/paper/2016/file/31857b449c407203749ae32dd0e7d64a-Paper.pdf>.
- [23] Jie Song, Bjoern Andres, Michael J Black, Otmar Hilliges, and Siyu Tang. End-to-end learning for graph decomposition. In *Proceedings of the IEEE/CVF International Conference on Computer Vision*, pages 10093–10102, 2019.
- [24] Naiyu Gao, Yanhu Shan, Yupei Wang, Xin Zhao, Yinan Yu, Ming Yang, and Kaiqi Huang. Ssap: Single-shot instance segmentation with affinity pyramid. In *Proceedings of the IEEE/CVF International Conference on Computer Vision*, pages 642–651, 2019.
- [25] Steffen Wolf, Alberto Bailoni, Constantin Pape, Nasim Rahaman, Anna Kreshuk, Ullrich Köthe, and Fred A Hamprecht. The mutex watershed and its objective: Efficient, parameter-free graph partitioning. *IEEE transactions on pattern analysis and machine intelligence*, 2020.
- [26] Thorsten Beier, Constantin Pape, Nasim Rahaman, Timo Prange, Stuart Berg, Davi D Bock, Albert Cardona, Graham W Knott, Stephen M Plaza, Louis K Scheffer, et al. Multicut brings automated neurite segmentation closer to human performance. *Nature methods*, 14(2):101–102, 2017.
- [27] Jan Funke, Fabian Tschopp, William Grisaitis, Arlo Sheridan, Chandan Singh, Stephan Saalfeld, and Srinivas C Turaga. Large scale image segmentation with structured loss based deep learning for connectome reconstruction. *IEEE transactions on pattern analysis and machine intelligence*, 41(7):1669–1680, 2018.

- [28] Bert De Brabandere, Davy Neven, and Luc Van Gool. Semantic instance segmentation with a discriminative loss function. *arXiv preprint arXiv:1708.02551*, 2017.
- [29] Davy Neven, Bert De Brabandere, Marc Proesmans, and Luc Van Gool. Instance segmentation by jointly optimizing spatial embeddings and clustering bandwidth. In *Proceedings of the IEEE/CVF Conference on Computer Vision and Pattern Recognition*, pages 8837–8845, 2019.
- [30] Alberto Bailoni, Constantin Pape, Steffen Wolf, Thorsten Beier, Anna Kreshuk, and Fred A Hamprecht. A generalized framework for agglomerative clustering of signed graphs applied to instance segmentation. *arXiv preprint arXiv:1906.11713*, 2019.
- [31] Leland McInnes and John Healy. Accelerated hierarchical density based clustering. In *2017 IEEE International Conference on Data Mining Workshops (ICDMW)*, pages 33–42. IEEE, 2017.
- [32] Dorin Comaniciu and Peter Meer. Mean shift: A robust approach toward feature space analysis. *IEEE Transactions on pattern analysis and machine intelligence*, 24(5):603–619, 2002.
- [33] Bjoern Andres, Thorben Kroeger, Kevin L Briggman, Winfried Denk, Natalya Korogod, Graham Knott, Ullrich Koethe, and Fred A Hamprecht. Globally optimal closed-surface segmentation for connectomics. In *European Conference on Computer Vision*, pages 778–791. Springer, 2012.
- [34] Kaiming He, Georgia Gkioxari, Piotr Dollár, and Ross Girshick. Mask r-cnn. In *Proceedings of the IEEE international conference on computer vision*, pages 2961–2969, 2017.
- [35] Marina Meilă. Comparing clusterings by the variation of information. In *Learning theory and kernel machines*, pages 173–187. Springer, 2003.
- [36] William M Rand. Objective criteria for the evaluation of clustering methods. *Journal of the American Statistical association*, 66(336):846–850, 1971.
- [37] Brian W Kernighan and Shen Lin. An efficient heuristic procedure for partitioning graphs. *The Bell system technical journal*, 49(2):291–307, 1970.
- [38] Tuomas Haarnoja, Aurick Zhou, Kristian Hartikainen, George Tucker, Sehoon Ha, Jie Tan, Vikash Kumar, Henry Zhu, Abhishek Gupta, Pieter Abbeel, and Sergey Levine. Soft actor-critic algorithms and applications. *CoRR*, abs/1812.05905, 2018. URL <http://arxiv.org/abs/1812.05905>.
- [39] Justin Gilmer, Samuel S. Schoenholz, Patrick F. Riley, Oriol Vinyals, and George E. Dahl. Neural message passing for quantum chemistry. *CoRR*, abs/1704.01212, 2017. URL <http://arxiv.org/abs/1704.01212>.
- [40] Olaf Ronneberger, Philipp Fischer, and Thomas Brox. U-net: Convolutional networks for biomedical image segmentation. *CoRR*, abs/1505.04597, 2015. URL <http://arxiv.org/abs/1505.04597>.
- [41] Richard S. Sutton and Andrew G. Barto. *Reinforcement Learning: An Introduction*. The MIT Press, second edition, 2018. URL <http://incompleteideas.net/book/the-book-2nd.html>.
- [42] Jörg Hendrik Kappes, Markus Speth, Björn Andres, Gerhard Reinelt, and Christoph Schn. Globally optimal image partitioning by multicuts. In Yuri Boykov, Fredrik Kahl, Victor Lempitsky, and Frank R. Schmidt, editors, *Energy Minimization Methods in Computer Vision and Pattern Recognition*, pages 31–44, Berlin, Heidelberg, 2011. Springer Berlin Heidelberg. ISBN 978-3-642-23094-3.
- [43] Lukas Biewald. Experiment tracking with weights and biases, 2020. URL <https://www.wandb.com/>. Software available from wandb.com.
- [44] Allam Shehata Hassanein, Sherien Mohammad, Mohamed Sameer, and Mohammad Ehab Ragab. A survey on hough transform, theory, techniques and applications. *CoRR*, abs/1502.02160, 2015. URL <http://arxiv.org/abs/1502.02160>.

- [45] D’Arcy Wentworth Thompson. *On Growth and Form*. Canto. Cambridge University Press, 1992. doi: 10.1017/CBO9781107325852.
- [46] Sourabh Bhide, Ralf Mikut, Maria Leptin, and Johannes Stegmaier. Semi-automatic generation of tight binary masks and non-convex isosurfaces for quantitative analysis of 3d biological samples, 2020.
- [47] Lucas von Chamier, Romain F Laine, Johanna Jukkala, Christoph Spahn, Daniel Krentzel, Elias Nehme, Martina Lerche, Sara Hernández-Pérez, Pieta K Mattila, Eleni Karinou, Séamus Holden, Ahmet Can Solak, Alexander Krull, Tim-Oliver Buchholz, Martin L Jones, Loïc A Royer, Christophe Leterrier, Yoav Shechtman, Florian Jug, Mike Heilemann, Guillaume Jacquemet, and Ricardo Henriques. Democratising deep learning for microscopy with ZeroCostDL4Mic. *Nature Communications*, 4 2021.
- [48] Adrian Wolny, Lorenzo Cerrone, Athul Vijayan, Rachele Tofanelli, Amaya Vilches Barro, Marion Louveaux, Christian Wenzl, Sören Strauss, David Wilson-Sánchez, Rena Lymbouridou, et al. Accurate and versatile 3d segmentation of plant tissues at cellular resolution. *Elife*, 9: e57613, 2020.
- [49] Bert De Brabandere, Davy Neven, and Luc Van Gool. Semantic instance segmentation with a discriminative loss function, 2017.
- [50] Reuben R. Shamir, Yuval Duchin, Jinyoung Kim, Guillermo Sapiro, and Noam Harel. Continuous dice coefficient: a method for evaluating probabilistic segmentations. *CoRR*, abs/1906.11031, 2019. URL <http://arxiv.org/abs/1906.11031>.

A Appendix

A.1 Method 2

In Method 2 the node features are not learned end-to-end by the agent, but instead generated as part of the environment; see also Figure 6. To this end, we employ self-supervised learning to generate a superpixel embedding, as explained in Section A.2. In case of a weak reward function, we find Method 2 preferable over Method 1 which jointly learns the node features. To generate a well performing agent with our method, the reward signal needs to be somewhat close to the "true" metric when evaluating a proposed segmentation. If it is close enough, e.g. by direct supervision or fairly specific priors such as the ones we use for the fruitfly dataset, we can use a weak state representation and learn how to extract the node features jointly (Method 1). Conversely, if the reward does not fit the "true" metric well, it is beneficial to remove the complexity of joint learning and provide a more informative state representation (Method 2).

A.2 Self-supervised pretraining

For self-supervised pre-training, we use a method based on the contrastive loss formulation of [49]. Consider a graph $G = (V, E)$, where the nodes in $V = \{1, 2, \dots, n\}$ correspond to the individual superpixels and the edges in $E = \{(i, j) | i \neq j \text{ and } i, j \in V\}$ connect nodes with adjacent superpixels. In addition, consider edge weights $W \in \mathbb{R}^{|E|}$ associated with every edge. Here, we infer the weights from pixel-wise boundary probability predictions and normalize the weights such that $\sum_{w \in W} w = 1$ holds. We train a 2D U-Net to predict embeddings for each node in V by pulling together pixel embeddings that belong to the same superpixel and pushing apart pixel embeddings for *adjacent* superpixels. The intensity of the push force is scaled by the weight of the respective edge. With pixel embeddings x_n and node embeddings $f_i = \frac{1}{m_i} \sum_{k \in s_i} x_k$, where m_i is the mass of the superpixel for node i and s_i is the set of indices for all pixels of the corresponding superpixel, and in accordance

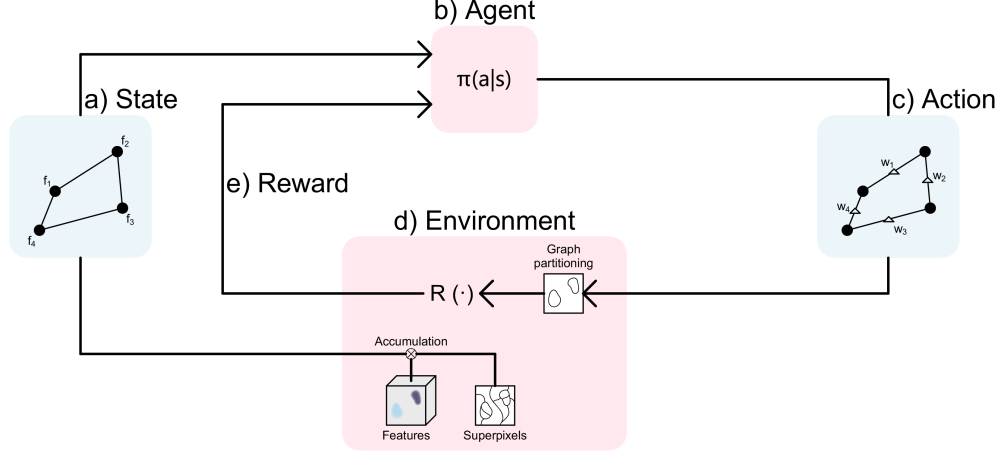


Figure 6: Interaction of the agent with the environment for Method 2: (a) shows the state which is composed of the superpixel graph where each node comes with a feature vector encoding features for the respective superpixel. This features are obtained by accumulation of pre-trained pixel-level features per superpixel; Given the state, the agent (b) predicts edge weights on the graph; These edge weights serve as the actions (c); the actions are processed by a graph partitioning algorithm which is part of the environment (d); (e) shows the rewards, based on the resulting segmentation. Rewards are obtained using a set of predefined and data dependent rules. The rewards are given back to the agent and the episode terminates.

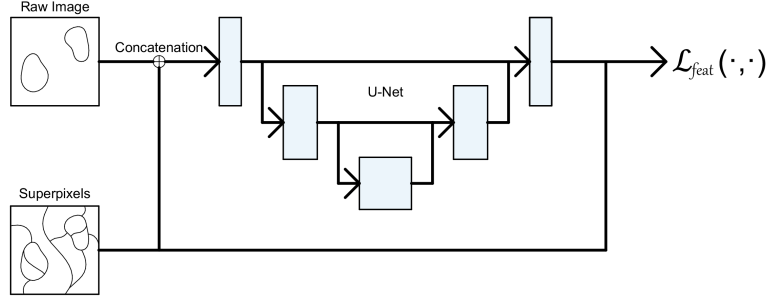


Figure 7: Training setup of the feature extractor. The input is a concatenation of the raw data and a smoothed edge map of the superpixels. The superpixel over-segmentation is used in the loss again as the supervision for learning the embedding space.

with [49] we formulate the loss as

$$\mathcal{L}_{var} = \frac{1}{|N|} \sum_{i=1}^{|N|} \frac{1}{m_i} \sum_{n=1}^{m_i} [d(f_i, x_n) - \delta_v]_+^2 \quad (12)$$

$$\mathcal{L}_{dist} = \sum_{(i,j) \in E} w_{(i,j)} [2\delta_d - d(f_i, f_j)]_+^2 \quad (13)$$

$$\mathcal{L}_{feat} = \mathcal{L}_{var} + \mathcal{L}_{dist} \quad (14)$$

Here $[\cdot]_+$ refers to selecting the max value from the argument and 0. The forces are hinged by the distance limits δ_{var} and δ_{dist} . $d(\cdot)$ refers to the distance function in the embedding space. Since the feature extractor is trained self-supervised, we give it a smooth edge map of the superpixels as well as the raw data as an input, see Figure 7.

The training of the feature extractor happens prior to training the agent, see also Section A.1.

A.3 Reward Generation

We seek to express the rewards based on prior rules derived from topology, shape, texture, etc. Rules are typically formulated per-object, Section A.8 describes the object-to-sub-graph reward mapping. The reward function is part of the environment and the critic learns to approximate it via Q-learning, enabling the use of non-differentiable functions.

This approach can also be extended to semantic instance segmentation where in addition to the instance labeling a semantic label is to be predicted. To this end, each predicted object is softly assigned to one of the possible classes and the reward is generated specifically for the predicted class. We make use of this extension by separating the objects into a foreground and background class in our experiments.

In addition to the sub-graph rewards our approach can also be extended to global rewards by global pooling of the output of the critic GNN and adding the squared difference of global action value and reward to Equation 4. Alternatively, the global reward can be distributed onto the sub-graph rewards via a weighted sum of sub-graph reward and global reward. In the second approach a different global reward can be specified per class in the case of the semantic instance segmentation formulation. We make use of the per class global reward to encode a reward for the correct number of predicted objects in our experiments.

The biggest challenge in designing the reward function is to avoid local optima. Since the reward is derived from each predicted object, we define the reward by extracting shape features, position, orientation and size of objects and compare them with our expectation of the true object’s features. This similarity score should be monotonically increasing as the objects fit our expectation better. All used similarity functions are to a certain extend linear, however an exponential reward function can speed up learning significantly. Consider an object level reward $r \in [0, 1]$, which is linear. We calculate the exponential reward by

$$r_{exp}(r) = \frac{\exp(r\theta)}{\exp(\theta)} \quad (15)$$

where the factor θ determines the range of the gradient in the output. We also find that it is better to compute the reward as a "distance function" of all relevant features rather than decomposing it into the features and simply summing up the corresponding rewards. In our experiments the latter approach behaved quite unpredictably and often generated local optima which the agent could not escape.

A.4 Object level rewards

We have tested generating the rewards based directly on the object scores instead of using the subgraph decomposition described in Section A.8. Since rewards are mainly derived from the features of the predicted objects it seems reasonable to formulate the supervision signal based directly on those objects. To this end we calculate a scalar reward per object as sketched in Figure 8. In this setting, the agent needs the information about the predicted objects when it learns from its own actions, which is in contradiction to the usual RL paradigm since the critic needs the predicted objects to predict the action values. However, the critic is not used during exploration where the objects for the explored actions are already available and can be used to predict action values. In this case, the critic uses a second GNN to predict the per-object action values. It is applied to an object’s subgraph, which is composed of all edges that have at least one node in common with the respective object. The graph convolutions are followed by a global pooling operation which yields the scalar action value. This GNN replaces the MLPs used in the case of the reward subgraph decomposition. After extensive testing, we found that this approach is always inferior to the subgraph decomposition.

A.5 Impact of different feature space capacities

In Table 2 we compare the performance of our method, using different numbers of dimensions in the space of the learned node features (the number of channels in the output of the feature extractor U-Net). We find that the reduced capacity of small feature spaces helps the agent perform better. Here we train and evaluate on the fruit fly embryo dataset.

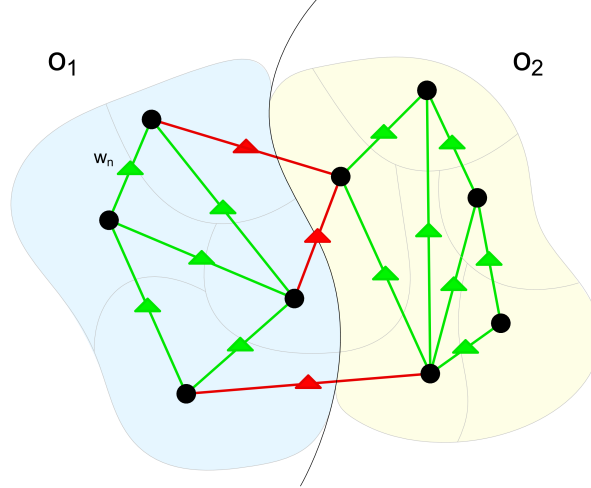


Figure 8: Object level rewards. We accumulate edge rewards over each object where we consider all edges that have at least one node within the respective object. E.g. for o_1 we consider all edges that are covered by the light blue object as well as all the red "unmerge" edges.

Table 2: Quantitative evaluation of our method using different feature space dimensionality. We use Symmetric Best Dice as well as the Variation of Information metric to compare all results on the validation set.

n feature channels	SBD	VI merge	VI split
4	0.518 ± 0.018	0.889 ± 0.081	0.823 ± 0.135
12	0.493 ± 0.026	0.821 ± 0.158	1.241 ± 0.220
16	0.482 ± 0.020	0.838 ± 0.118	1.374 ± 0.357

A.6 Random seed evaluation

Figure 9 shows the training evolution of the average subgraph reward from different random seeds. The model performance depends on the chosen seed and for the final comparisons we select the runs based on the best score. The seed is generated randomly on each run.

A.7 Gaussian weighting scheme

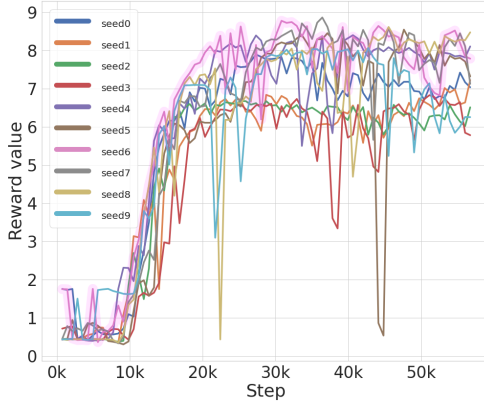
Figure 10 shows the Gaussian weighting scheme which was used to generate the rewards for the fruitfly embryo data. It can be seen as a very approximate semantic segmentation and serves the purpose of generating a reward maximum at the very approximate segmentation without using it.

A.8 Randomly generated subgraphs

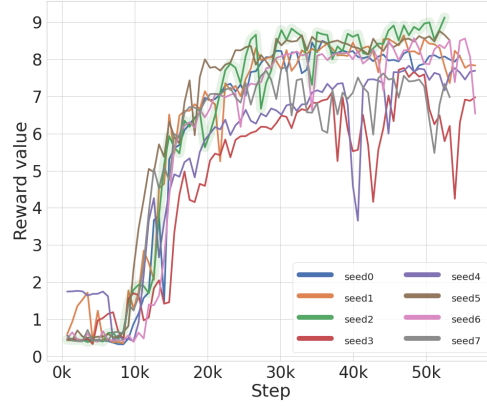
We select subgraphs using Algorithm 1. Subgraphs are selected randomly starting from random nodes and continuously adding edges to the subgraph until the desired size is reached. The size of the subgraph is defined by the number of edges in the graph. Algorithm 1 selects edges such that the subgraphs are connected and such that their density is high (low number of nodes in the subgraph).

A.9 Multistep Reinforcement Learning

We tested several methods that use multiple steps within one episode. In this formulation we predict the changes starting from an initial state rather than predicting absolute values for the edge weights. For example, we can start from a state defined by edge weights derived from a boundary map. Given that this state should be somewhat close to the desired state we expect that a few small steps within one episode should be sufficient. In our experiments, we have typically used three steps per episode



(a) Setup 1. Features of size 16. 10 seeds.



(b) Setup 2. Features of size 12. 8 seeds.

Figure 9: Running the same setup from different random seeds reveals a stable stride for high rewards. We select the model for comparison based on the best achieved reward (magenta line in Fig. 9a and green line in Fig. 9b) which makes the training/validation process completely independent on any ground truth annotations.

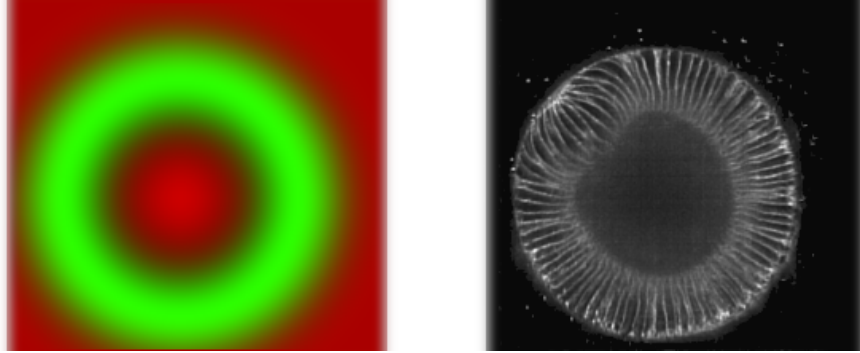


Figure 10: Weighting scheme for object rewards and merge affinity rewards, roughly encoding foreground location. Left: weights for object rewards in green and for merge affinity rewards in red, both are Gaussian and concentric. Right: an example of an underlying real image.

and used actions that can change the weight per edge by the values in $[-0.1, 0.1]$. This approach generates an action space that is exponentially larger than in the stateless formulation. A priori this setup might still be more stable because it is not possible to diverge from a given solution so fast due to the incremental changes per step.

Let us first consider the case with groundtruth edge weights. In this case, we can give an accurate reward not only for the final segmentation but for every step. Hence, the path to the optimal state is linear. Take for example an initial edge with weight 0.3 and its respective ground truth edge with weight 0. We can give a reward that mirrors the correct confidence of the action by using the negative value of the predicted action: $r = -a$. This allows us to set the discount factor *gamma* of the RL setup to 0, because the path to the correct edge weight is linear and the correct direction will be encoded in the reward at every step. Therefore the rewards for the following steps are not needed. Setting the discount to 0 generates a problem of equal size as the stateless RL method. However, for this approach the ground truth direction of the path must be known for each edge, so it can only be used in the case of full supervision.

To generalize the multistep approach to the rule based rewards we need to choose a different setup where a constant reward is given at each non terminal step and the rule based one is given at the terminal step. This setup requires a discount factor $\gamma > 0$ and has an action space more complex than

Algorithm 1: Dense subgraphs in a rag

Data: $G = (V, E)$, l **Result:** subgraphs by sets of l edges

```
1 Initialization:  $SG = \emptyset$ ;  
2 while  $E \setminus SG \neq \emptyset$  do  
3    $pq = \text{PriorityQueue}$ ;  
4    $prio = 0$ ;  
5    $n\_draws = 0$ ;  
6    $sg = \emptyset$ ;  
7    $sg_{vtx} = \emptyset$ ;  
8    $i, j = (ij)$  s.t.  $(ij) \in E \setminus SG$ ;  
9    $pq.push(i, prio)$ ;  
10   $pq.push(j, prio)$ ;  
11   $sg = sg \cup (ij)$ ;  
12   $sg_{vtx} = sg_{vtx} \cup i$ ;  
13   $sg_{vtx} = sg_{vtx} \cup j$ ;  
14  while  $|sg| < l$  do  
15     $n, n\_prio = pq.pop()$ ;  
16     $n\_draws++$ ;  
17     $adj = \{(nj) | \exists (nj) \in E \text{ and } \exists j \in sg_{vtx}\}$ ;  
18    forall  $(nj) \in adj$  do  
19       $sg = sg \cup (nj)$ ;  
20       $n\_draws = 0$ ;  
21    if  $|adj| < deg(n)$  then  
22       $n\_prio -= (|adj| - 1)$ ;  
23       $pq.push(n, n\_prio)$ ;  
24    if  $pq.size() \leq n\_draws$  &  $\exists j | (nj) \in E, j \notin sg_{vtx}$  then  
25       $j \in \{j | (nj) \in E, j \notin sg_{vtx}\}$ ;  
26       $prio++$ ;  
27       $pq.push(j, prio)$ ;  
28       $sg = sg \cup (nj)$ ;  
29       $sg_{vtx} = sg_{vtx} \cup j$ ;  
30   $SG = sg \cup SG$   
31 return  $SG$ 
```

the stateless approach, because future steps are necessary to compute the reward. We tested this setup extensively against the stateless approach and found that it was not competitive.

A.10 Hyper-parameters and network details

For U-Net, we use the standard implementation with features maps size of 32, 64, and 128. The backbone for both actor and critic are GNNs. In addition, the critic employs different MLPs, one for each subgraph size. Most of the hyperparameters for actor, critic and U-Net are chosen empirically and given in the configuration files in the main repository.

The source code with brief instructions is posted on Anonymized GitHub ¹. The dataset is available on a general-purpose open-access repository Zenodo ².

A.11 Direct supervision

The aim of this project has been to find a way to train a segmentation algorithm from not-necessarily-differentiable rules, priors and expectations for the segmented objects. Looking ahead to the next stages, we have also qualitatively evaluated the behavior of our setup in case direct supervision such

¹https://anonymous.4open.science/r/nips_paper_rlforseg/

²<https://zenodo.org/record/4899944#.Y0RWq0xRVEZ>

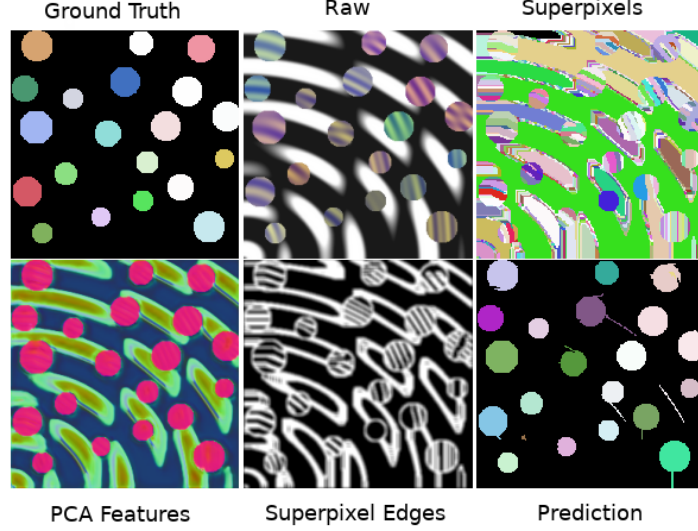


Figure 11: An example of a fully supervised prediction on the "Circles" dataset. This was obtained with use of the Dice score over subgraphs as a fully supervised reward using Method 1. We initialized the feature extractor U-Net with the pretrained embeddings from Subsection 4.1. It is interesting to see how the features for the circles are emphasized a lot more after training.

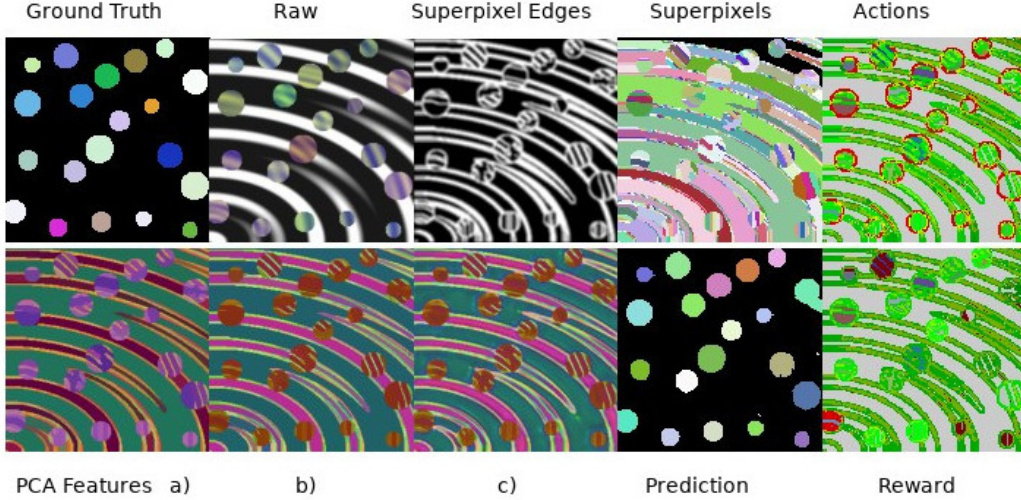


Figure 12: An example for prediction with mixed supervision on the "Circles" dataset. The reward was defined as follows: we use for all but for one image the unsupervised CHT reward and for one image we make use of ground truth and the Dice score as the reward. We find that this mixed reward setting leads to improved performance compared to the unsupervised CHT reward.

as fully segmented images is available. We tried both full supervision (Fig. 11) and mixed supervision, using one fully segmented image and also the prior rules (Fig. 12). Under full supervision with a set of ground-truth edge weights, we compute the the Dice Score [50] of the predicted edge weights a and the ground-truth \hat{a} for each sub-graph and use it as reward. We find this function to be robust by class imbalance present in our setup. In both cases, the agent learns to segment the circles correctly, demonstrating fast and robust convergence. Note, how learned pixel features converge to a state which strongly resembles a semantic segmentation of the image.